Supplemental Digital Content

Lung Metabolic Activation as an Early Biomarker of ARDS and Local Gene Expression Heterogeneity

Figures

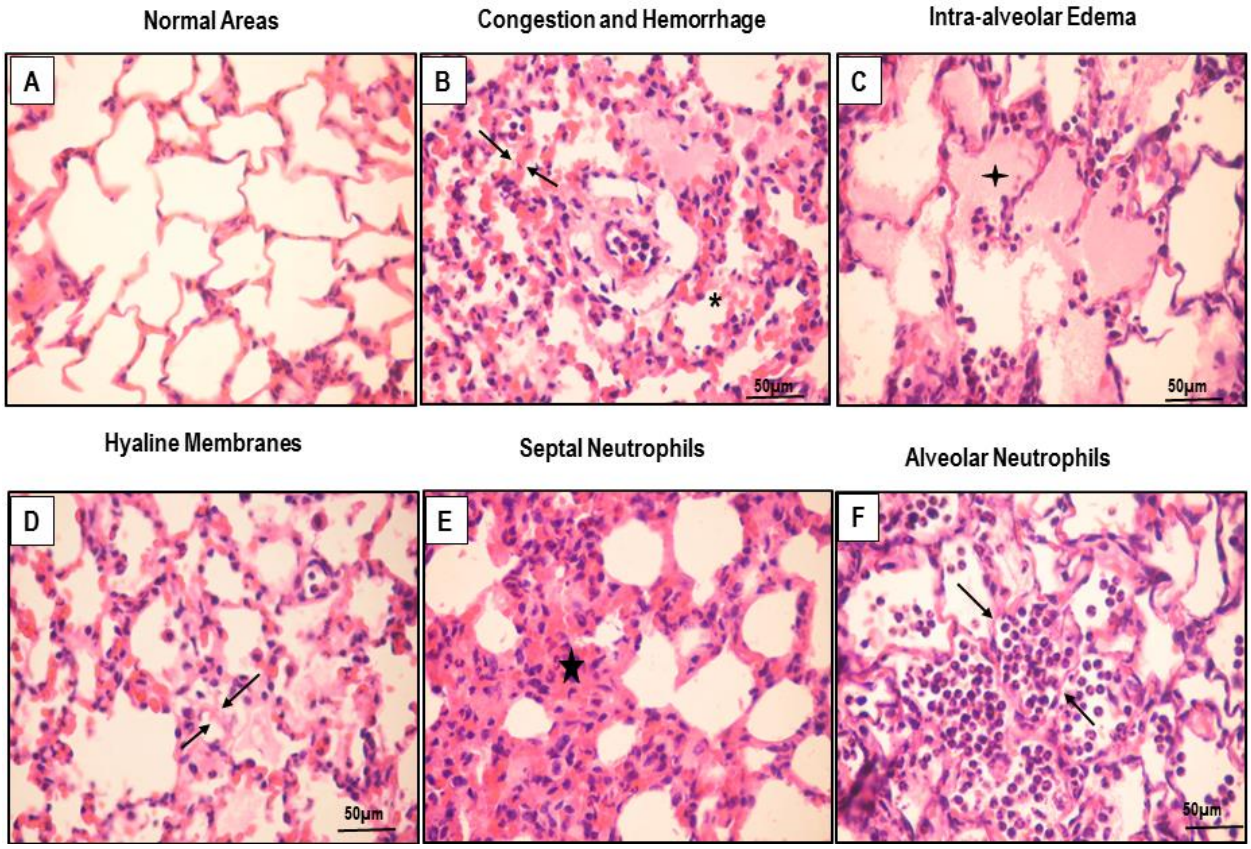

Fig. S1. Optical H&E microscopy of lung parenchyma after 20 hours of mechanical ventilation and endotoxemia. Whereas normal areas are still present in lung parenchyma (**A**), a number of regions already show findings consistent with progress to diffuse alveolar damage. These include: **B**) capillary congestion (arrows) with various amount of hemorrhage (*); **C**) intra-alveolar edema (✦), the earliest light microscopy change together with capillary congestion and hemorrhage; **D**) hyaline membranes, the histologic hallmark of the acute stage of diffuse alveolar damage, is seen as homogeneous amorphous eosinophilic structures (arrows) plastered along the alveolar septa; (**E** and **F**) prominent interstitial inflammatory cell infiltrate consisting predominantly of neutrophils, first of all along of the alveolar septa (**E**) and then inside alveoli (**F**).

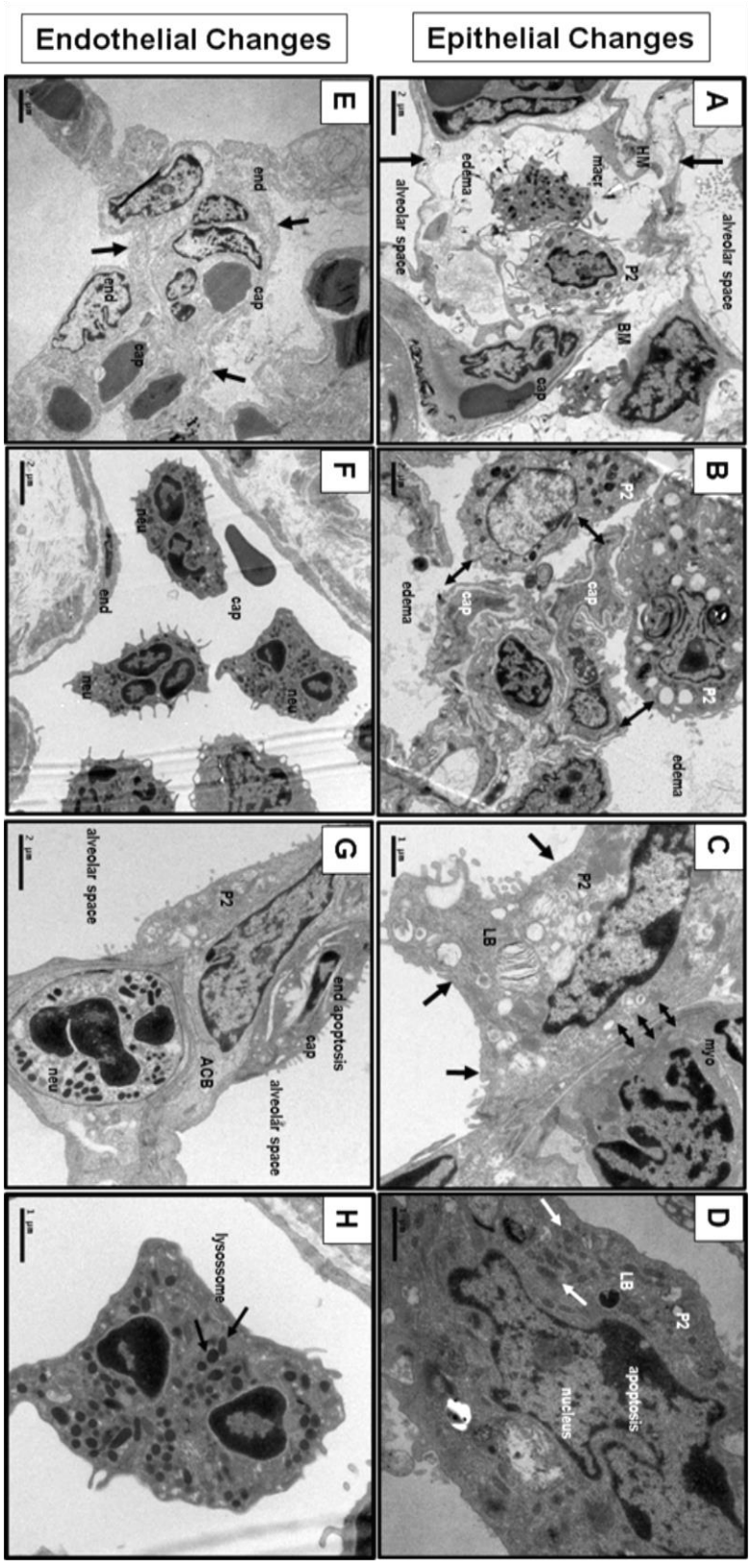
Endothelial Changes
Epithelial Changes
A
alveolar space
HM
edema
P2
BM
cap
alveolar space
B
P2
cap
edema
P2
edema
C
P2
LB
myo
D
P2
LB
apoptosis
nucleus
E
end
cap
end
cap
F
neu
cap
neu
end
neu
G
end apoptosis
cap
alveolar space
P2
ACB
alveolar space
neu
H
lysosome

Fig. S2. Electron microscopy of alveolar capillary barrier (ACB) after 20 hours of mechanical ventilation and endotoxemia. A and E) epithelium (P2) lining airspaces and endothelium lining the capillaries (cap) in an interstitial layer (two arrows) housing the connective tissue fibers. The earliest electron microscope changes in acute lung injury consist of prominent interstitial edema (edema), followed by sloughing of alveolar lining cells (P2), denudation of the epithelial basement membrane (BM) and nuclear debris with fibrin forming the hyaline membrane (HM). B) Cytoplasmic swelling of epithelial (P2) and endothelium (end) contributes for detachment between alveolar epithelium cells and capillaries (two arrows) as well as surface irregularities in epithelium and endothelial cells (two arrows). C) Apposition of collapsed alveoli (three arrows) determines interstitial thickening (single arrows). D) Degenerative changes in alveolar epithelial cells (P2) are characterized by nuclear apoptosis (apoptosis), cytoplasmic swelling, lamellar bodies (LB) decrease and enlarged mitochondria with irregularity of the internal cristae (arrows). A and F) inflammatory cells consisting predominantly of macrophages (macr) in alveolar spaces (A) and recruitment of numerous neutrophils (neu) inside capillaries and small vessels (F). G) endothelial apoptosis (end apoptosis) and neutrophils outside the capillary and inside the interstitial layer. H) numerous lysosomes in activated neutrophils outside the pulmonary capillary demonstrating their state of activation and cellular structural readiness for protease release.

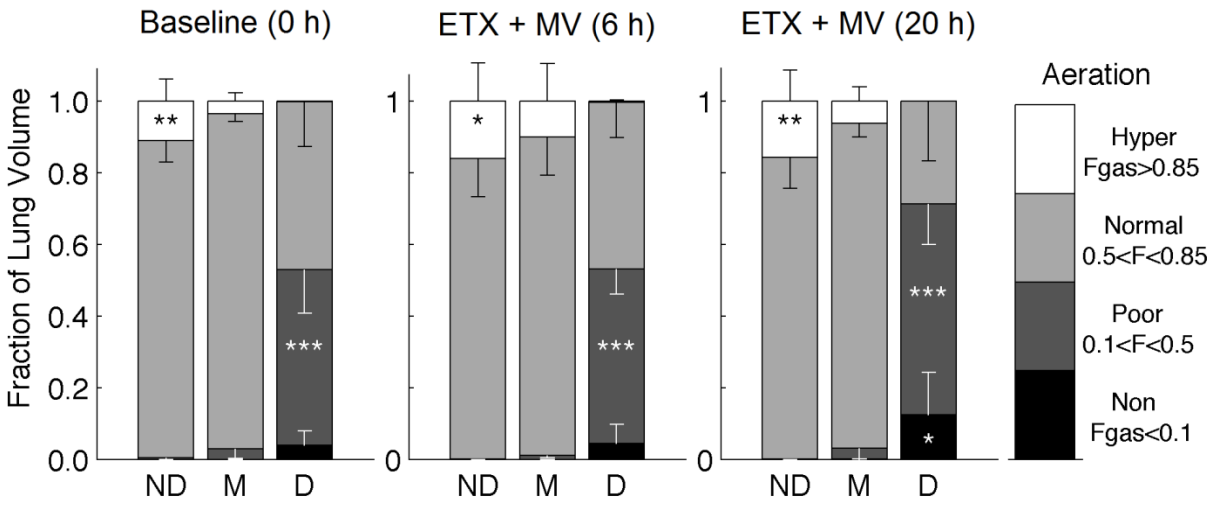

Fig. S3. Time trends of regional aeration compartments. Aeration compartments in non-dependent (ND), middle (M), and dependent (D) lung regions at 0, 6, and 20 h time points. While most of the lung fell within the normal aeration range (light gray bars), non-dependent regions contained hyper-inflated volume (white bars) throughout the experiments, and dependent regions showed substantial poorly-aerated (dark gray bars) and non-aerated volume (black bars) at all time points. *p<0.05, **p<0.01, ***p<0.001 for ND versus D at each time point.

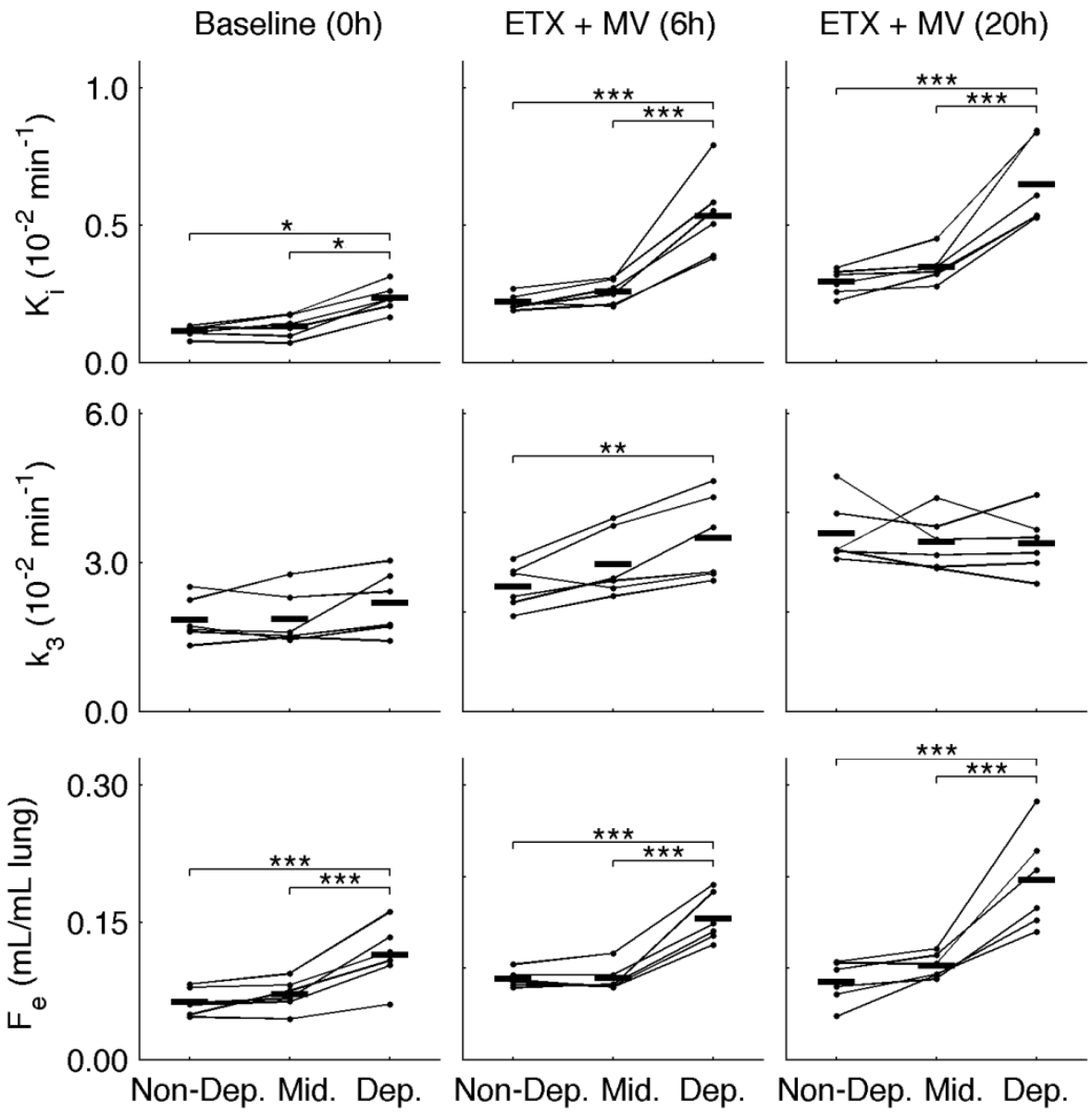

Fig. S4. Topographical trends in the ^{18}F-FDG net uptake rate (K_i), phosphorylation rate (k_3), and extravascular volume of distribution (F_e) over 20 h of early experimental ARDS. *p<0.05, **p<0.01, ***p<0.001 for differences between regions

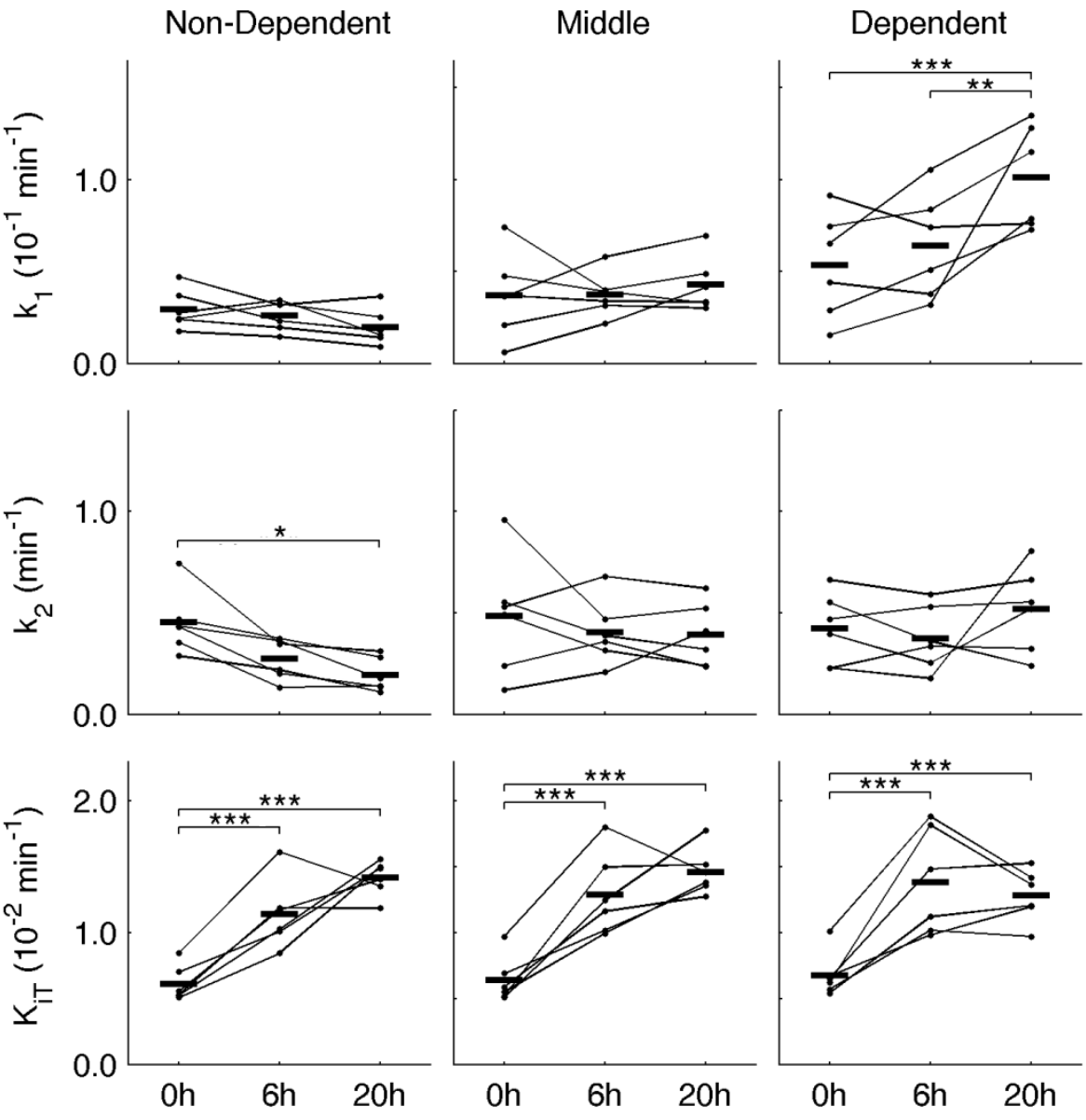

Fig. S5. Regional trajectories of the plasma-to-extravascular transport rate constant (k_1), the extravascular-to-plasma transport rate constant (k_2), and the tissue-normalized net uptake rate of ^{18}F-FDG (K_{iT}) over 20 h of early experimental ARDS. K_{iT} showed significant changes during the first 6 h in all regions, but no further changes from 6 to 20 h. *p<0.05, **p<0.01, ***p<0.001 for changes between respective time points.

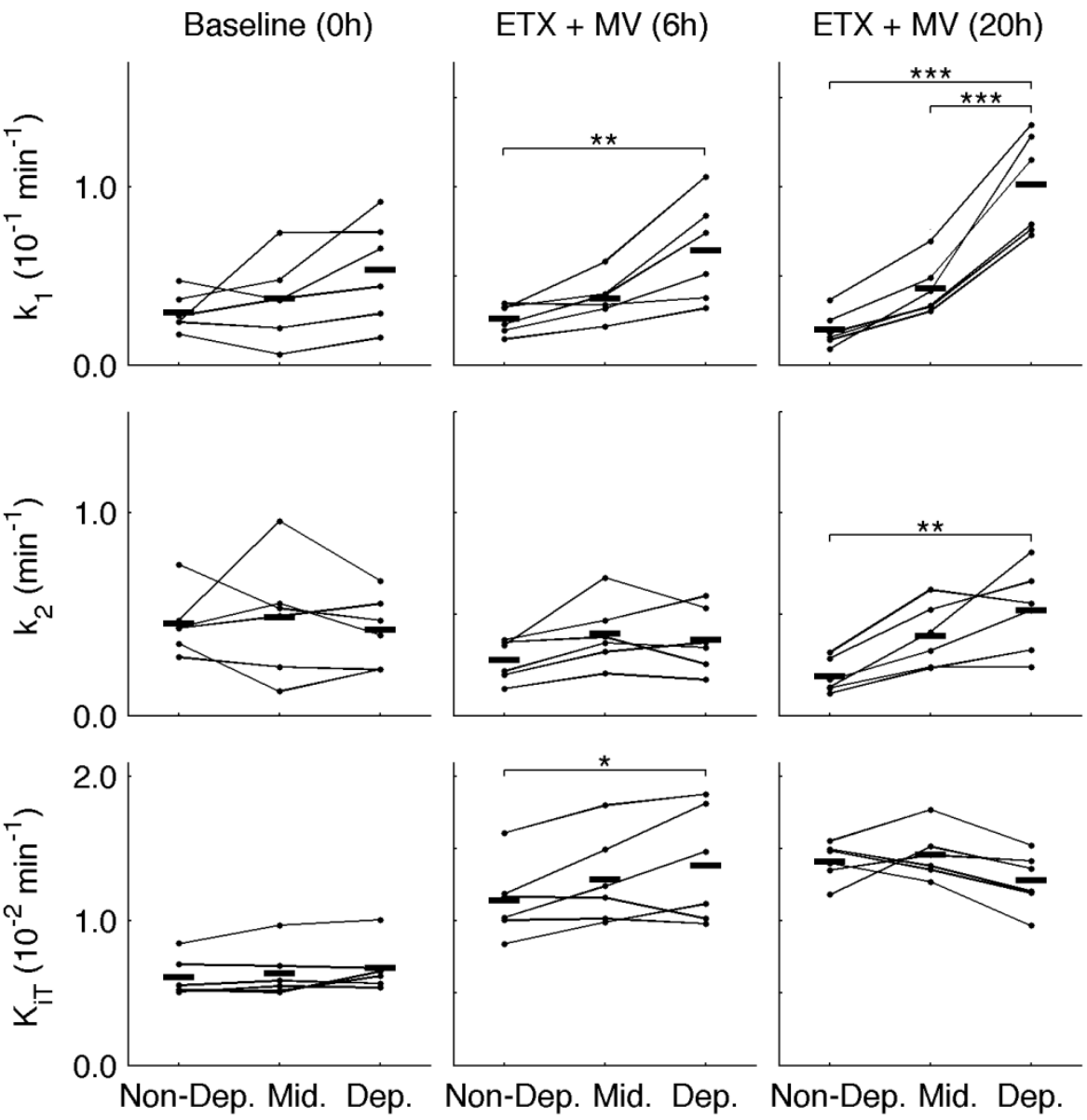

Fig. S6. Topographical trends in the plasma-to-extravascular transport rate constant (k_1), the extravascular-to-plasma transport rate constant (k_2), and the tissue-normalized net uptake rate of ^{18}F-FDG (K_{iT}) over 20 h of early experimental ARDS. K_{iT} showed regional differences only at the 6 h time point, with homogeneously elevated K_{iT} values observed at 20 h. *p<0.05, **p<0.01, ***p<0.001 for differences between regions

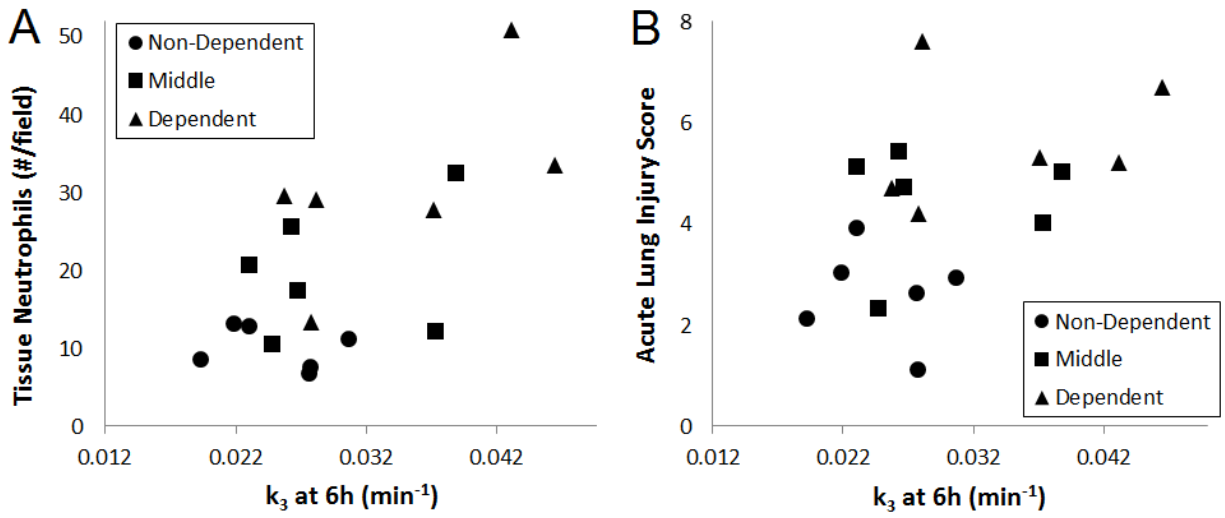

Fig. S7. Histological measures of neutrophilic inflammation (A) and lung injury (B) measured regionally in lung tissue after 20 h of early experimental ARDS were correlated with the regional ^{18}F-FDG phosphorylation rate (k_3) measured at 6h. Correlations were statistically significant for both neutrophil numbers per field (**A**, $r=0.65$, $p<0.01$) and acute lung injury score (**B**, $r=0.47$, $p<0.05$). These findings highlight the potential value of regional measurements of k_3 for the prediction of local injury progression.

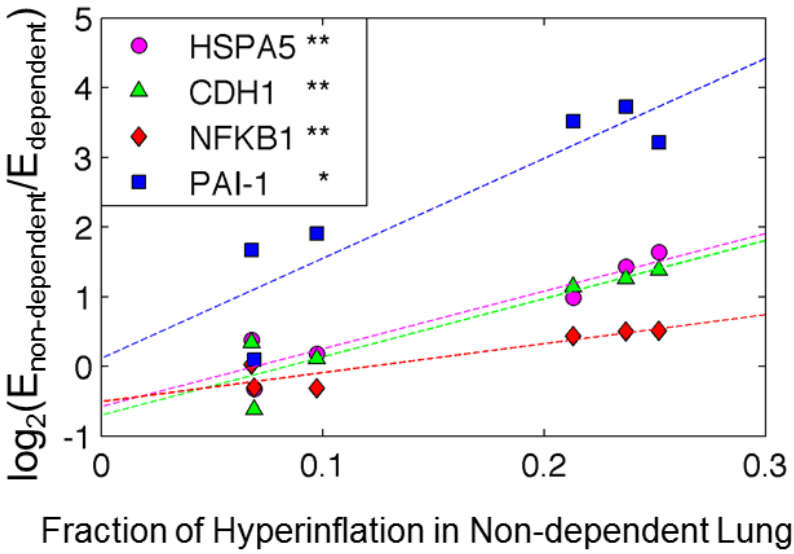

Fig. S8. Association of non-dependent (ventral) differential expression of VILI-associated genes with hyperinflation in non-dependent regions. Each of these genes showed higher relative expression in non-dependent regions compared to dependent regions for higher levels of hyperinflation in the non-dependent lung. Expression ratios were derived from microarray results. Hyperinflation in the non-dependent lung was defined as the fraction of voxels in the non-dependent region with $F_{GAS}>0.85$ at the 6h time point. * $p<0.05$, ** $p<0.01$ for Pearson correlation between variables

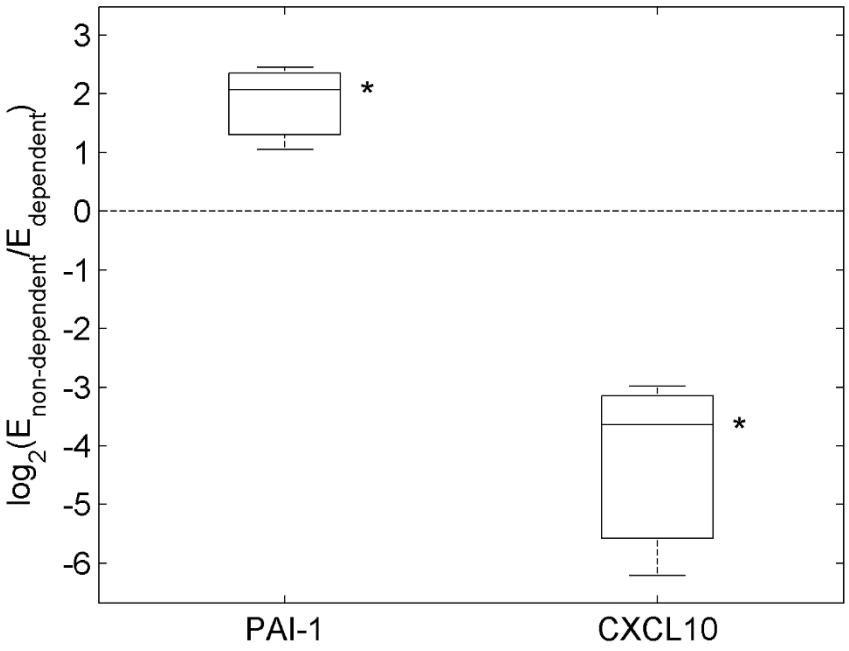

Fig. S9. Real-time polymerase chain reaction (RT-PCR) validation of microarray gene expression results. In 3 of the 6 studied sheep, tissue samples from non-dependent (ventral) and dependent (dorsal) regions were also used for RT-PCR validation of microarray results. The genes with the most significant differential expression in non-dependent (PAI-1) and dependent (CXCL10) regions were measured. Duplicate measurements were made, and for each animal the non-dependent-to-dependent expression ratios were averaged. The PCR results corroborated the microarray findings, with significantly higher PAI-1 expression in non-dependent regions and higher CXCL10 expression in dependent regions. * $p<0.05$ for expression ratios different from 0

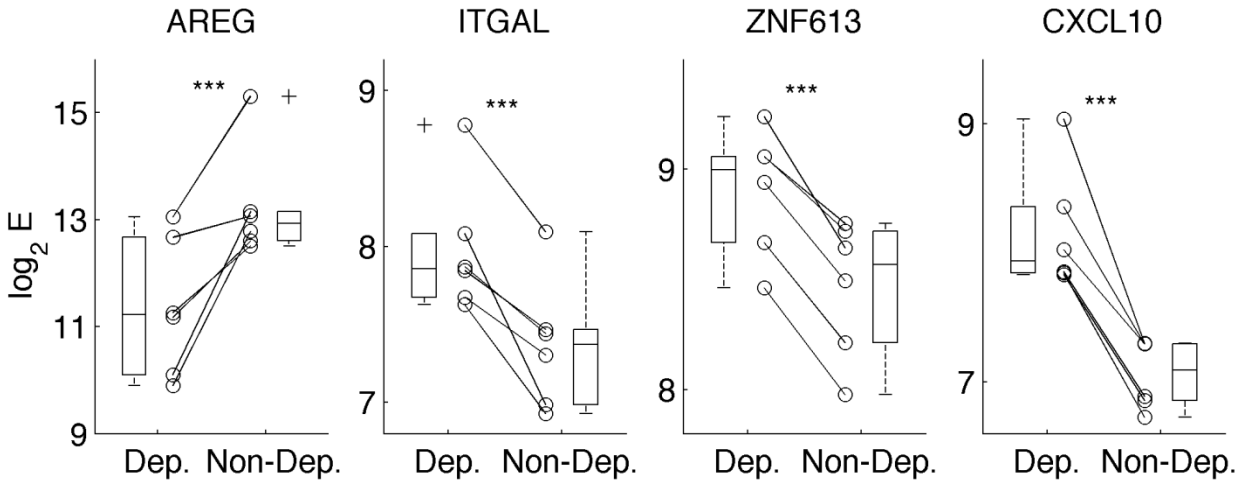

Fig. S10. Paired comparisons in genes of large intra-regional expression variability. Several genes showed notable variability in expression between animals, but paired comparisons allowed for identification of significant differential expression between non-dependent and dependent regions of the lung. ***p<0.001 for difference between dependent and non-dependent expression

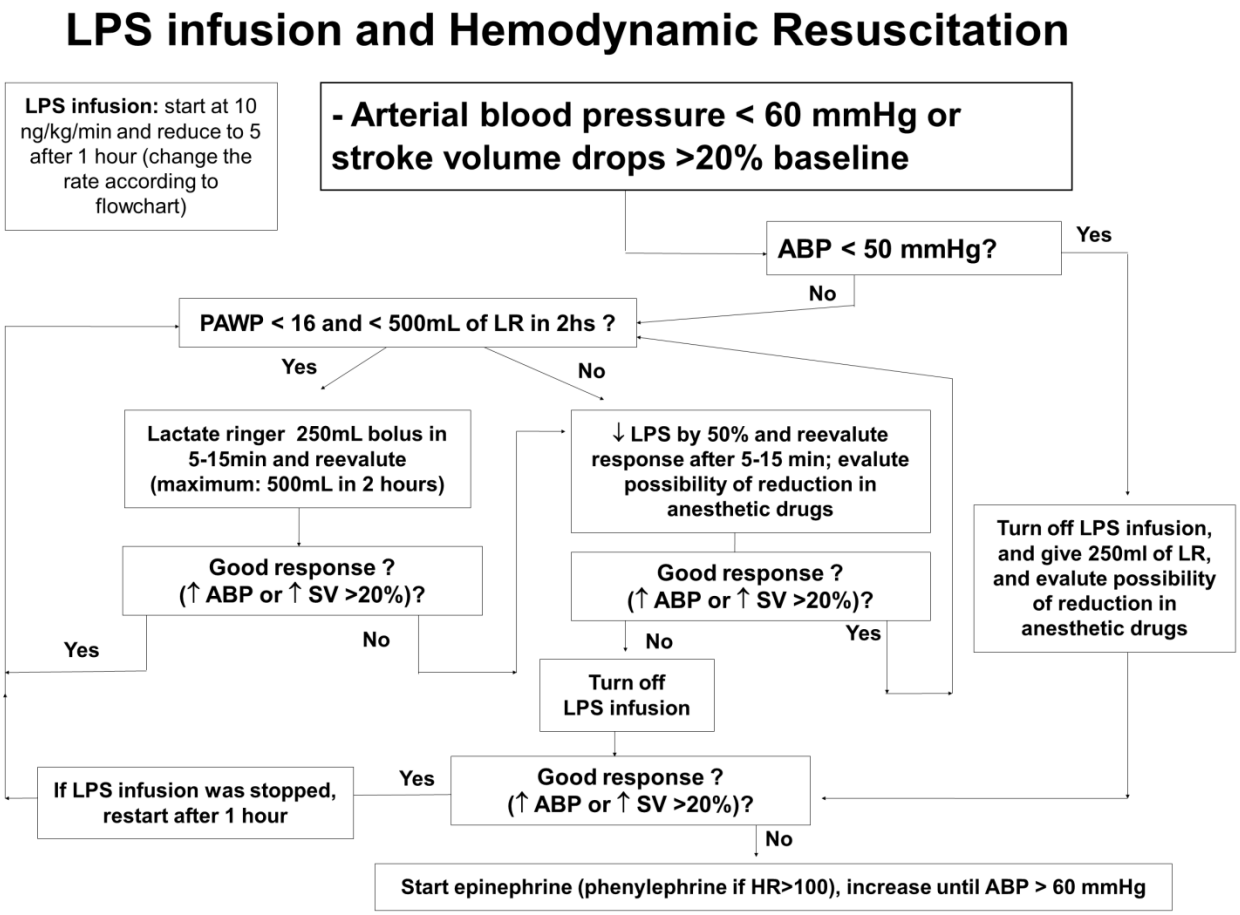

Fig. S11. Algorithm for hemodynamic management and adjustment of endotoxin infusion rate.

Table S1 – Peripheral white blood cell counts at baseline and after 6 and 20h of mechanical ventilation and endotoxemia.

	Baseline (n=6)	**6h (n=6)**	**20h (n=6)**	**P**
WBC ($10^3 \cdot \mu L^{-1}$)	9.2 ± 2.6	8.4 ± 3.8	10.5 ± 2.7	0.34
Neutrophil ($10^3 \cdot \mu L^{-1}$)	1.8 (1.4 – 2.3)*	0.3 (0.2 – 0.7)¶	2.2 (0.8 – 3.6)	0.03
Lymphocyte ($10^3 \cdot \mu L^{-1}$)	6.5 ± 2.1	7.8 ± 3.4	7.6 ± 1.7	0.48
Monocyte ($10^3 \cdot \mu L^{-1}$)	0.9 ± 0.2*	0.2 ± 0.1¶	0.6 ± 0.2	0.01

Variables are expressed as mean ± SD for normally distributed variables and median and interquartile range (25 – 75%) otherwise. * $p \leq 0.05$ (Baseline vs. 6h), and ¶ $p \leq 0.05$ (6h vs. 20h). WBC = white blood cell.

Table S2 – Histologic variables in the whole lung, non-dependent and dependent regions after 20h of mechanical ventilation and endotoxemia.

Light microscopy	**Whole lung**	**Non-dependent**	**Dependent**
Total neutrophil (%)	20.2 ± 7.5	20.8 ± 17.2	19.5 ± 7.6
Alveolar neutrophil (%)	17.3 ± 7.8	18.1 ± 16.6	16.4 ± 6.7
Septal neutrophil (%)	25.3 ± 7.1	25.7 ± 17.7	24.8 ± 8.8
Hyaline membrane (%)	7.1 ± 4.3	7.7 ± 8.2	6.5 ± 5.3
Edema (%)	8.4 ± 4.1	8.9 ± 8.3	7.9 ± 4.7
Transmission electron microscopy	**Whole lung**	**Non-dependent**	**Dependent**
Alveolar capillary membrane	1.9 (1.6 – 2.0)	2.0 (1.3 – 2.4)	1.5 (1.0 – 2.0)
Mitochondria	1.5 (1.1 – 1.9)	1.0 (1.0 – 2.5)	1.5 (1.0 – 2.0)
Endoplasmic reticulum	1.1 (1.0 – 1.3)	1.3 (1.0 – 1.5)	1.0 (1.0 – 1.0)*
Lysosomes	1.0 (1.0 – 1.4)	1.0 (1.0 – 1.8)	1.0 (1.0 – 1.0)

Variables are expressed as mean ± SD for normally distributed variables and median and interquartile (25-75%) otherwise. *P < 0.05 for non-dependent *vs.* dependent regions.

Table S3 – Gene ontologies related to lung injury for the set of genes with significant differential regional expression at $p<0.01$ as measure by microarray analysis (174 total annotated genes included).

Ontology Term	p value
regulation of leukocyte activation	0.000011
regulation of cytokine production	0.013
regulation of apoptosis	0.024
immune response	0.00038

Ontology terms were derived using the DAVID bioinformatics software (reference 21 in manuscript).